Novel Size-Independent Modeling of the Dilute Solution Conformation of the Immunoglobulin IgG Fab′ Domain Using SOLPRO and ELLIPS

Beatriz Carrasco,* Jose Garcia de la Torre,* Olwyn Byron,# David King,§ Chris Walters,# Susan Jones,¶ and Stephen E. Harding#

*Departamento de Quimica Fisica, Facultad de Quimica, Universidad de Murcia, 30071 Murcia, Spain; #National Centre for Macromolecular Hydrodynamics, University of Nottingham, School of Biological Sciences, Sutton Bonington LE12 5RD, England; §Celltech Therapeutics, Bath Road, Slough, Berkshire, England; and ¶Biomolecular Structure and Modelling Unit, Department of Biochemistry and Molecular Biology, University of London, London WC1 6BT, England

ABSTRACT The proliferation of hydrodynamic modeling strategies to represent the shape of quasirigid macromolecules in solution has been hampered by ambiguities caused by size. Universal shape parameters, independent of size, developed originally for ellipsoid modeling, are now available for modeling using the bead-shell approximation via the algorithm SOLPRO. This paper validates such a "size-independent" bead-shell approach by comparison with the exact hydrodynamics of 1) an ellipsoid of revolution and 2) a general triaxial ellipsoid (semiaxial ratios a/b, b/c) based on a fit using the routine ELLIPSE (Taylor et al., 1983. *J. Mol. Graph.* 1:30–38) to the chimeric (human/mouse) IgG Fab′ B72.3; a similar fit is obtained for other Fabs. Size-independent application of the bead-shell approximation yields errors of only ~1% in frictional ratio based shape functions and ~3% in the radius of gyration. With the viscosity increment, errors have been reduced to ~3%, representing a significant improvement on earlier procedures. Combination of the Perrin frictional ratio function with the experimentally measured sedimentation coefficient for the same Fab′ from B72.3 yields an estimate for the molecular hydration of the Fab′ fragment of ~(0.43 ± 0.07) g/g. This value is compared to values obtained in a similar way for deoxyhemoglobin (0.44) and ribonuclease (0.27). The application of *SOLPRO* to the shape analysis of more complex macromolecules is indicated, and we encourage such size-independent strategies. The utility of modern sedimentation data analysis software such as SVEDBERG, DCDT, LAMM, and MSTAR is also clearly demonstrated.

INTRODUCTION

There are two approaches to the modeling of quasirigid macromolecules in dilute solution, using hydrodynamic and solution scattering-based methodologies. One is the whole-body or ellipsoid approach (Perrin, 1934, 1936; Harding, 1989); the other is the multiple-sphere array or bead approach (Bloomfield et al., 1967; Garcia de la Torre and Bloomfield, 1981; Garcia de la Torre, 1989). Although with the latter the hydrodynamic theory is approximate rather than exact, it does allow the prospect of representations of complex structures such as antibodies (Byron, 1992). With either type of approach one of the key difficulties to be confronted is that of molecular volume: experimental hydrodynamic coefficients such as the sedimentation coefficient and diffusion coefficient (manifestations of the translational frictional characteristics of a macromolecule), or the intrinsic viscosity (bulk flow characteristics), radius of gyration (mass distribution characteristics about the centre of mass), molecular covolume (thermodynamic nonideality), or rotational diffusion decay times (rotational friction) all depend on the volume properties of a molecule as well as shape; in fact in many cases the shape contribution is secondary to molecular volume.

To facilitate this move away from the ambiguities caused by size-dependent approaches, "size-independent" or "universal" hydrodynamic shape functions have now been developed for both modeling strategies. Indeed, this has been used for ellipsoid modeling since the 1930s; for example, Perrin's (1936) "translational frictional ratio due to shape" or P function (Harding and Rowe, 1982a,b, 1983) or Simha's (1940) "viscosity increment" or ν function. A suite of algorithms for the PC has recently been made available (Harding et al., 1997) for ellipsoids of revolution (ELLIPS1, direct prediction of axial ratios from a user-specified shape function) and the much more general triaxial ellipsoids (ELLIPS2, rigorous evaluation of the complete set of hydrodynamic shape functions for user-specified triaxial dimensions or (two) axial ratios; ELLIPS3,4, for combining hydrodynamic measurements to evaluate the triaxial shape of a molecule). These size-independent shape functions are known as "universal" shape functions, and Table 1 lists them and the experimental parameters from which they are derived. Some, such as P and ν, require an estimate for the degree of solvent association or "hydration"; some combined functions such as β, R, Π, and Λ_h do not.

Bead modeling would appear to benefit strongly from such a size-independent approach, particularly with regard to the considerable uncertainties/ambiguities concerning the volume of a particle and the volume of the beads. So the

Received for publication 8 December 1998 and in final form 13 August 1999.

Address reprint requests to Dr. Stephen E. Harding, NCMH Unit, University of Nottingham, Sutton Bonington LE12 5RD, England. Tel.: 44-115-951-6148; Fax: 44-115-951-6142; E-mail: steve.harding@nottingham.ac.uk.

Dr. Byron's present address is Division of Infection and Immunity, Institute of Biomedical and Life Sciences, University of Glasgow, Glasgow G12 8QQ, Scotland.

0006-3495/99/12/2902/09 $2.00

TABLE 1 Universal hydrodynamic parameters

Universal hydrodynamic parameter	Name	Experimental parameters required for its measurement
ν	Viscosity increment	Intrinsic viscosity $[\eta]$, partial specific volume ν, molecular hydration δ
P	Perrin translational frictional ratio	Translational diffusion coefficient D (or sedimentation coefficient s and molecular weight M), $\bar{\nu}$, δ
R	Wales–van Holde R-function	Sedimentation concentration dependence ("Gralen") parameter k_s, $[\eta]$
β	Scheraga-Mandelkern function	D (or s and M), $\bar{\nu}$, $[\eta]$
u_{red}	Reduced excluded volume	Thermodynamic 2nd virial coefficient B, M, $\bar{\nu}$, δ, charge (valency) Z, ionic strength I
Π	Pi-function	B, M, $[\eta]$, Z, I
G	G-function	Radius of gyration, M, $\bar{\nu}$*
$\theta_{+,-}$	Reduced electrooptic decay constant	Electrooptic decay constants times, $\theta_{+,-}$; M, $\bar{\nu}$,
$\delta_{+,-}$	Electrooptic delta shape functions	$\theta_{+,-}$, M, $\bar{\nu}$, $[\eta]$
$\gamma_{+,-}$	Electrooptic gamma shape functions	s (or D), $\theta_{+,-}$, M, $\bar{\nu}$
τ_h/τ_0	Harmonic mean fluorescence anisotropy depolarization time ratio	Harmonic mean fluorescence anisotropy depolarization time; M, $\bar{\nu}$, δ
Ψ_h	Psi-function	Harmonic mean fluorescence anisotropy depolarization time; M, $\bar{\nu}$, s (or D)
Λ_h	Lambda-function	Harmonic mean fluorescence anisotropy depolarization time; M, $\bar{\nu}$, $[\eta]$
τ_i/τ_0 (i = 1–5)	Time-resolved fluorescence anisotropy relaxation time ratio	Time-resolved fluorescence anisotropy relaxation time; M, $\bar{\nu}$, δ
Λ_i (i = 1–5)	Time-resolved lambda function	Time-resolved fluorescence anisotropy depolarization times; M, $\bar{\nu}$, $[\eta]$
Ψ_i (i = 1–5)	Time resolved psi function	Time-resolved fluorescence anisotropy depolarization times; M, $\bar{\nu}$, s (or D)

*If the density of bound water is the same as free, then $\nu \approx \bar{\nu}$.

algorithm SOLPRO (Garcia de la Torre et al., 1997) was constructed for precisely this reason, as well as to provide improved estimates for rotational and scattering-based parameters. A more recent version of the algorithm (Garcia de la Torre et al., 1999) also permits the prediction of NMR-based relaxation times as well as molecular covolumes for general particles.

Shell modeling

In the conventional application of bead modeling the volume occupied by the particle is filled with spheres of various sizes; the number of beads required is minimized by making them as large as possible. Thus taking the case, for example, of an ellipsoid of revolution, this can be modeled as a straight string of beads whose radii decrease from the center, tapering toward the ends (Bloomfield et al., 1967; Garcia de la Torre and Bloomfield, 1977). An inconvenience of this procedure is that the (relative) size of some beads may be quite large and close to the size of the full particle. In this way, one or a few beads dominate the hydrodynamic behavior of the model, and this has the consequence that the rotational coefficients and the intrinsic viscosity (or viscosity increment) are more or less affected. The origin of the problem and its solution, in the form of the so-called volume corrections, has already been described (Garcia de la Torre and Rodes, 1983; Garcia de la Torre and Carrasco, 1998).

Very recently, an alternative procedure has been proposed to avoid such problems (Carrasco, 1998; Carrasco and Garcia de la Torre, 1999). The hydrodynamic model does not fill the particle's volume; instead it is just the particle's surface that is represented by a shell constructed with many small identical beads. The shell-model procedure was actually proposed in the early work of Bloomfield et al. (1967). The serious drawback of shell modeling is that the number of frictional elements in the model is very large, and the calculations require large amounts of CPU time. Methods for building such models and for rigorously computing their solution properties have been devised; for the details, see Carrasco (1998) and Carrasco and Garcia de la Torre (1999). Indeed, it has been shown by these authors that the hydrodynamic properties of ellipsoids of revolution can be accurately reproduced by such a shell approach.

In this paper we focus on five aspects of molecular modeling in solution, based on the IgG Fab′ fragment (Fig. 1):

1. Calculating the triaxial ellipsoid shape (of semiaxes a, b, c, with $a > b > c$ and axial ratios a/b, b/c) from the crystal structure of the chimeric (humanized mouse) IgG Fab′ known as B72.3 (King et al., 1992; Brady et al., 1992), using the routine ELLIPSE (Taylor et al., 1983), and then comparing this shape with that from the crystal structure of human, mouse, and another chimeric IgG Fab′.

2. Evaluating the exact set of universal hydrodynamic parameters for this shape, using the routine ELLIPS2 (Harding et al., 1997).

3. Comparing this set of data with that for the equivalent prolate ellipsoid of revolution approximation to this structure (where b and c are set equal).

4. Comparing these data with a bead-shell model approximation of this ellipsoid of revolution to validate this approximation for subsequent modeling for more complex structures involving several domains, with each domain

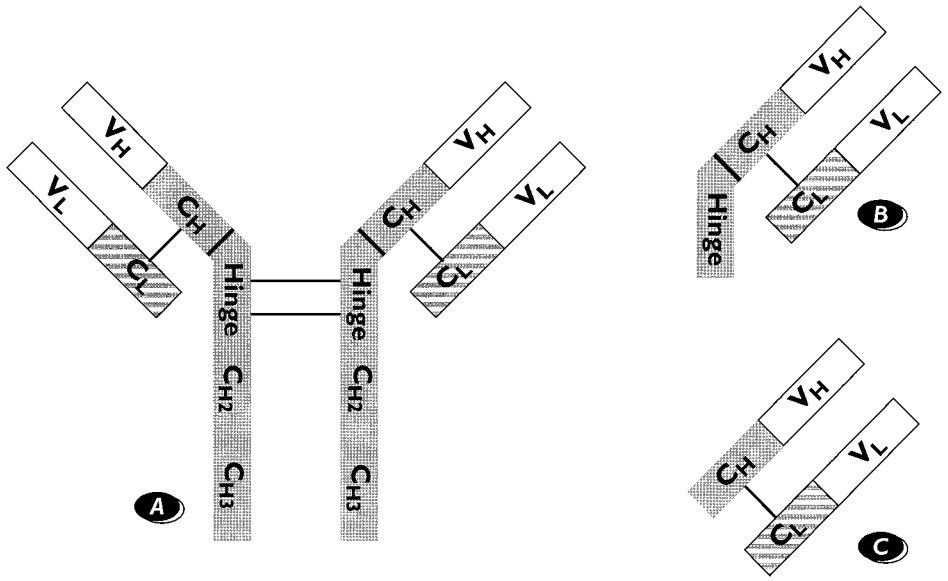

FIGURE 1 Schematic Fab′ (B72.3 IgG). (*A*) Intact antibody. (*B*) Fab′ fragment. (*C*) Fab fragment.

represented first by an ellipsoid and then by the equivalent bead-shell model.

5. Combination of the bead-shell/ellipsoid value for P with the experimentally measured frictional ratio (from the sedimentation coefficient) for the Fab′ fragment of B72.3 Fab′ (King et al., 1992; Brady et al., 1992); this is used to estimate the molecular hydration of the Fab′ molecule. Having estimated the hydration and validated the bead-shell approach in this way for the Fab′ domain, we can then use this to provide a sound basis for further studies representing the conformation of intact immunologically active molecules.

Triaxial shape of IgG Fab′ and Fab

An objective method for defining the triaxial shape of a protein molecule from its atomic structural coordinates has been provided by Taylor et al. (1983). This method, which is insensitive to small deviations from an ideal ellipsoidal form, is based on the inertial, momental, or "Cauchy" ellipsoid (see MacMillan, 1936; Synge and Griffin, 1959), dilated so that it forms a close approximation to the protein surface. The original procedure, recently implemented by Hubbard (1994) in a FORTRAN algorithm, is used to calculate the ratios of the principal axes of the equimomental ellipsoid for the 3D coordinates of a protein. These ratios can be used in conjunction with a second algorithm, SURFNET (Laskowski, 1995), to generate a 3D surface representation of the ellipsoid; the combined algorithm is referred to as ELLIPSE. Fig. 2 *A* shows the fit to the crystal structure for chimaeric B72.3c Fab′ with (a/b, b/c) = (1.595, 1.418). Table 2 compares the corresponding axial ratios (a/b, b/c)'s for this protein with the chimeric Fab hA5B7, and wild-type human and mouse Fab fragments. It is clear that there is little species variation in Fab′ or Fab (gross) shape, based on the published crystal coordinates.

Comparison of the triaxial ellipsoid shape of IgG Fab′ with a prolate ellipsoid approximation

Table 3 compares the exact hydrodynamic parameters for a triaxial ellipsoid of axial ratios (a/b, b/c) = (1.595, 1.418) with those of the equivalent prolate ellipsoid, whose minor axes are taken to be equal to the mean of b and c, giving a revised (a/b, b/c) of ~(1.83, 1.0). Both sets of data—exact to four significant figures—were evaluated using the program ELLIPS2 (Harding et al., 1997). It can be seen that the ellipsoid of revolution approximation leads to errors of ~1% in the frictional ratio-based P function and ~4% in both the intrinsic viscosity-based ν function and the radius of gyration-based G function and only leads to serious error (~10% or above) in the rotational diffusion-based γ_+ and γ_- functions; because with the frictional ratio-based P function this can be experimentally measured to a precision no better than ±1%, such an approximation is therefore a reasonable one.

Comparison with bead-shell model

Fig. 2 *B* shows the bead-shell model approximation to the surface of this ellipsoid of revolution. The final column of Table 3 gives the set of universal parameters calculated from SOLPRO for this model.

The procedure for arranging the beads is as follows: a number of small beads of radius σ are placed in such a way that their centers lie on the surface of the ellipsoid. Each bead is touching its closest neighbors, or closely tangent to them, with small gaps. The number of beads, N, is large and increases with decreasing σ; for instance, for the smallest radius considered in our calculations, σ = 3.2 Å (which is a fraction $0.04a$ of the longest semiaxis, a = 80 Å, of the ellipsoid), we have N = 874. The computing time for the HYDRO calculation of the shell model grows as N^3. Actu-

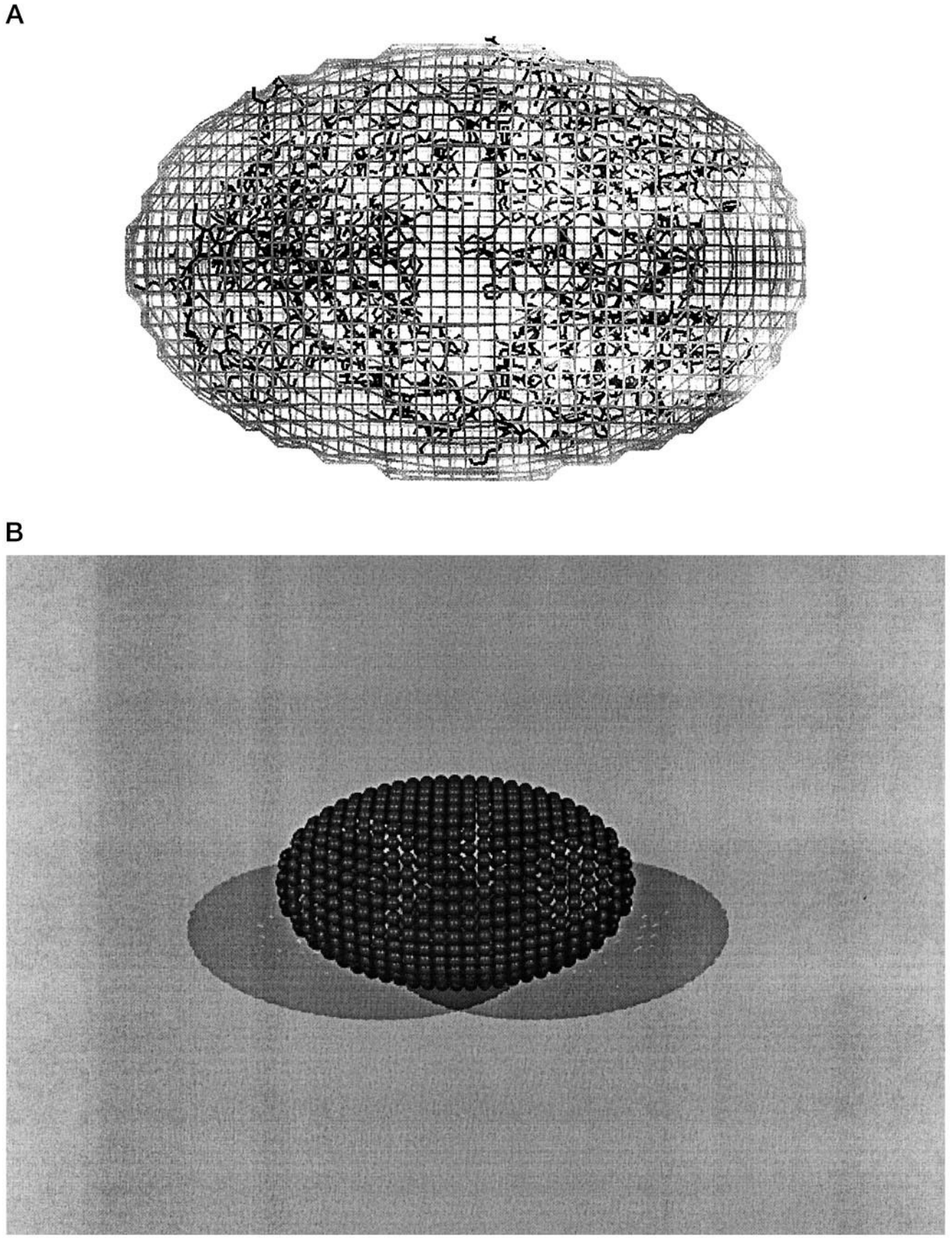

FIGURE 2 (*A*) Shape models for B72.3 Fab′ triaxial ellipsoid fit to the crystal structure using PROTRUDER and SURFNET and (*B*) bead-shell model for the equivalent prolate ellipsoid using SOLPRO.

TABLE 2 Triaxial shape of IgG Fab′ or Fab fragments from crystal structures

Fab′/Fab	{*a/b, b/c*}	PDB file	Reference
B72.3c Fab′	1.60, 1.42	1bbj-(3.1 Å)	Brady et al. (1992)
Human Fab	1.59, 1.36	8Fab-human-(1.8 Å)	Saul and Poljak (1992)
Murine Fab	1.68, 1.39	1aif-mouse-(2.9 Å)	Ban et al. (1995)
hA5B7 Fab	1.65, 1.40	1ad0-(2.5 Å)	Banfield et al. (1997)

Ellipsoid semi axes, $a > b > c$. Axial ratios, {*a/b, b/c*}.

ally, we have made the calculations for various bead sizes, ranging from $0.112a$ to $0.04a$. The resulting properties show a slight dependence on σ; the final results are obtained by extrapolating to the shell-model limit of $\sigma = 0$. This is done by fitting the data to a polynomial of degree 1 or 2, depending on the cases. With the HYDRO evaluations completed before SOLPRO, the universal parameters are then evaluated (Table 3).

TABLE 3 Comparison of hydrodynamic parameters for an ellipsoidal particle of axial ratios (*a/b, b/c*) = (1.595, 1.418) with ellipsoid of revolution and shell approximations

Hydrodynamic parameter (universal shape function)	Exact value	Prolate ellipsoid approximation (*a/b, b/c* = 1.83, 1.0)	Shell-bead model approximation
ν	2.907	2.802 (−3.6%)	2.729 (−2.6%) [−6.1%]
P	1.045	1.033 (−1.1%)	1.023 (−0.97%) [−2.2%]
R	1.474	1.501 (+1.8%)	1.517 (+1.0%) [+2.8%]
$10^{-6} \times \beta$	2.124	2.123 (−0.05%)	2.125 (+0.01%) [+0.005%]
u_{red}	9.131	8.809 (−3.5%)	—
Π	3.141	3.144 (+0.10%)	—
G	0.7473	0.715 (−4.3%)	0.697 (−2.5%) [−6.7%]
θ_+^{red}	0.1655	0.1749 (+5.4%)	—
θ_-^{red}	0.1138	0.1200 (+5.2%)	—
δ_+	2.887	2.940 (+1.8%)	—
δ_-	1.984	2.017 (+1.6%)	—
γ_+	1.689	1.516 (−10%)	—
γ_-	1.160	1.040 (−10%)	—
τ_h/τ_0	1.194	1.131 (−5.3%)	1.118 (−1.2%) [−6.8%]
Ψ_h	0.9854	0.9919 (+0.66%)	0.986 (−0.59%) [+0.06%]
Λ_h	2.436	2.479 (+1.7%)	2.441 (−1.6%) [+0.20%]
τ_1/τ_0	1.007	0.9531 (−5.7%)	0.972 (+1.9%) [−3.5%]
τ_2/τ_0	1.305	1.247 (−4.4%)	1.209 (−3.0%) [−7.4%]
τ_3/τ_0	1.326	1.247 (−5.9%)	1.209 (−3.0%) [−8.8%]
τ_4/τ_0	1.465	1.389 (−5.2%)	1.317 (−5.2%) [−10%]
τ_5/τ_0	1.007	0.9531 (−5.7%)	0.972 (+1.9%) [−3.5%]
Λ_1	2.887	2.940 (+1.80%)	2.809 (−4.5%) [−2.7%]
Λ_2	2.228	2.248 (+0.89%)	2.256 (+0.35%) [+1.2%]
Λ_3	2.192	2.248 (+2.5%)	2.256 (+0.35%) [+2.8%]
Λ_4	1.984	2.017 (+1.6%)	2.027 (+0.49%) [+2.1%]
Λ_5	2.887	2.940 (+1.8%)	2.809 (−4.5%) [−3.5%]
Ψ_1	1.043	1.050 (+0.67%)	1.033 (−1.6%) [−0.97%]
Ψ_2	0.9566	0.9601 (+0.36%)	0.966 (+0.61%) [+0.97%]
Ψ_3	0.9515	0.9601 (+0.90%)	0.966 (+0.61%) [+1.5%]
Ψ_4	0.9203	0.9261 (+0.63%)	0.933 (+0.74%) [+1.4%]
Ψ_5	1.043	1.0500 (+0.67%)	1.033 (−1.6%) [−0.96%]

Figures in parentheses: in the prolate ellipsoid column these represent the percentage error compared with the true value for the triaxial ellipsoid; in the shell-bead column those in ( ) represent the percentage error compared with the ellipsoid of revolution model; those in [ ] represent the total percentage error compared with the triaxial ellipsoid.

To assess the usefulness of this approximation we have given in parentheses ( ) the percentage error compared with the ellipsoid of revolution model; those in square brackets [ ] represent the total percentage error compared with the triaxial ellipsoid. Let us now consider each in turn.

1. Ability of the bead-shell model to satisfactorily model the ellipsoid of revolution (curved parentheses). The shell model gives excellent reproduction with the viscosity increment ν only 2.6% out, the radius of gyration G function at 2.5%, and the frictional ratio P function less than a percent. Reproducibility of the other functions is also excellent, including the particularly useful R (1%) and L_h (1.6%) functions, both of which are "hydration independent"; i.e., they do not require an assumed or measured value for the hydration δ to experimentally determine the function.

2. Comparison of the final result for the shell-bead model with the original triaxial ellipsoid value (square brackets). Despite the accumulation of error in the prolate ellipsoid approximation to the triaxial ellipsoid and then the shell-bead model to the prolate ellipsoid, reproducibility is very good, with ν, G, and P performing to within ~6%, 7%, and 2%, respectively, and R and L_h to within ~3% and ~0.2%, respectively (the latter assisted by a fortuitous cancellation). These results clearly vindicate both the bead-shell approach and the SOLPRO algorithm.

EXPERIMENTAL

Fab′

The Fab′ fragment of the chimeric antibody B72.3 was expressed directly in CHO cells as previously described (King et al., 1992). Fab′ was purified from the CHO cell supernatant, using affinity chromatography with mucin-sepharose. Submaxillary mucin acts as a mimic of the tumor-associated antigen recognized by B72.3 (Hanisch et al., 1989). Bovine submaxillary mucin was coupled to cyanogen bromide-activated Sepharose by standard techniques, packed into a column, and equilibrated with phosphate-buffered saline. CHO cell supernatant was applied directly to the column, which was then washed with phosphate-buffered saline before bound material was eluted with 0.1 M citric acid. The pH of eluted material was immediately adjusted to pH 6–7, and the purity was tested by sodium dodecyl sulfate-polyacrylamide gel electrophoresis. Purified material was demonstrated to be >95% pure after this single-step purification.

For sedimentation analysis the protein was dissolved in a standard phosphate chloride buffer (Green, 1933) of pH 6.8, $I = 0.10$.

Analytical ultracentrifugation

An Optima XL-A analytical ultracentrifuge (Giebeler, 1992) from Beckman Instruments (Palo Alto, CA) was employed to perform both sedimentation velocity and sedimentation equilibrium measurements. Solute distributions at 20.0°C were recorded via their UV absorption at 278 nm.

Sedimentation velocity

A rotor speed of 49,000 rev/min was employed. Sedimentation coefficients in the buffer at 20°C, $s_{T,b}$, were evaluated using SVEDBERG (Philo, 1997), LAMM (Behlke and Ristau, 1997), and DCDT (Stafford, 1992). These routines also yield estimates for the translational diffusion coeffi-

TABLE 4 Sedimentation and related parameters for Fab′

	$s^0_{20,w}$ (S)	M (g/mol)	$\bar{v}$ (ml/g)	f/f_0	δ (P = 1.045)	δ_{app} (P = 1.023)
B72.3 Fab′	3.92 ± 0.01	47,500	0.727	1.22 ± 0.01	0.43 ± 0.07	0.51 ± 0.07

cient, $D_{T,b}$. $s_{T,b}$ values were corrected to standard solvent conditions, the density, ρ, and viscosity, η, of water at 20°C, using the formula (Schachman, 1959)

$$s_{20,w} = \{(1 - \bar{v}\rho)_{20,w}/(1 - \bar{v}\rho)_{T,b}\} \cdot \{\eta_{T,b}/\eta_{20,w}\} \cdot s_{T,b} \quad (1a)$$

$\bar{v}$ is the partial specific volume, calculated from the amino acid sequence as 0.727 ml/g, using the consensus formula of Perkins (1986).

A similar correction was employed for the translational diffusion coefficient:

$$D_{20,w} = \{293.15/T\}/ \cdot \{\eta_{T,b}/\eta_{20,w}\} \cdot D_{T,b} \quad (1b)$$

where in this case T = 293.15K. $s_{20,w}$ values were plotted against sedimenting concentration (corrected for radial dilution) and extrapolated to infinite dilution according to the method of Schachman (1959):

$$s_{20,w} = s^0_{20,w}(1 - k_s c) \quad (2a)$$

where k_s is the Gralen (1944) parameter. A similar extrapolation was performed for translational diffusion:

$$D_{20,w} = D^0_{20,w}(1 + k_D c) \quad (2b)$$

In general the concentration dependence of D is much less pronounced (see, e.g., Harding and Johnson, 1985a,b).

Sedimentation equilibrium

The low/intermediate speed method was employed (Creeth and Harding, 1982). Equilibrium rotor speeds of 12,000 rpm were employed in 12-mm Yphantis-type multichannel cells. Only the radially innermost two channels were used, each with 80 μl of solution (dialysate in the solvent sector). Equilibrium was established within 36 h. Solute distributions at equilibrium were analyzed by the model-independent routine MSTARA (Cölfen and Harding, 1997); the apparent whole-cell weight-averaged molecular weight $M_{w,app}$ was extracted from the limiting value at the cell base of the M^* function (Creeth and Harding, 1982). A low loading concentration was used (0.5 mg/ml); at this concentration nonideality effects can be assumed to be negligible, and hence $M_{w,app} \approx M_w$.

RESULTS

Ultracentrifugation of Fab′

Analytical ultracentrifugation was performed on the Fab′ fragment of B72.3 to 1) assess the monodispersity, 2) confirm the monomeric state (solution molecular weight), 3) determine the sedimentation coefficient and the corresponding frictional ratio (f/f_o), 4) combine f/f_o with the Perrin (1936) function P values of Table 3 calculated from the crystal structure of the IgG Fab′ to obtain an estimate for the molecular hydration δ of the Fab′ molecule.

Confirmation of monodispersity and absence of self-association phenomena

This was supported by 1) the observation of only single boundaries from sedimentation velocity (Fig. 3), 2) no evidence of an increase in sedimentation coefficients with increase an in concentration (Fig. 4 *A*), 3) linear sedimentation equilibrium plots of log (absorbance) versus the radial displacement squared parameter ξ defined by

$$\xi = (r^2 - r_a^2)/(r_b^2 - r_a^2) \quad (3)$$

where r is the radial displacement from the rotor center and r_a, r_b are the radial positions of the cell meniscus and base, respectively.

Absolute molecular weight, M_w

Extrapolation of the M^* function to the cell base (Fig. 5) yielded a whole-cell weight-averaged molecular weight M_w = (47,000 ± 1000) g/mol, in virtually exact agreement with the sequence molecular weight of 47,499 g/mol calculated from the amino acid sequence. The result is also in agreement with the sedimentation-diffusion result; $s^o_{20,w}$ and $D^o_{20,w}$ values of (3.92 ± 0.01) × 10^{-13} s and (7.1 ± 0.2) × 10^{-7} cm^2 s^{-1} were obtained (Fig. 4). Combination via the Svedberg equation (Svedberg and Pedersen, 1940)

$$M_w = \{s^0_{20,w}/D^0_{20,w}) \cdot \{RT/(1 - \bar{v}\rho)\} \quad (4)$$

where R is the gas constant, yields a value for the molecular weight M_w of (49,000 ± 2000) g/mol, in good agreement.

Sedimentation coefficient and frictional ratio

The sedimentation coefficient $s^o_{20,w}$ is related to molecular shape via the frictional coefficient, f:

$$s^0_{20,w} = M(1 - \bar{v}\rho)/(N_A \cdot f) \quad (5)$$

where M is the molecular weight and N_A is Avogadro's number. Because f is also dependent on the molecular weight, the following more convenient representation is usually given; it uses instead of f the ratio of f to the

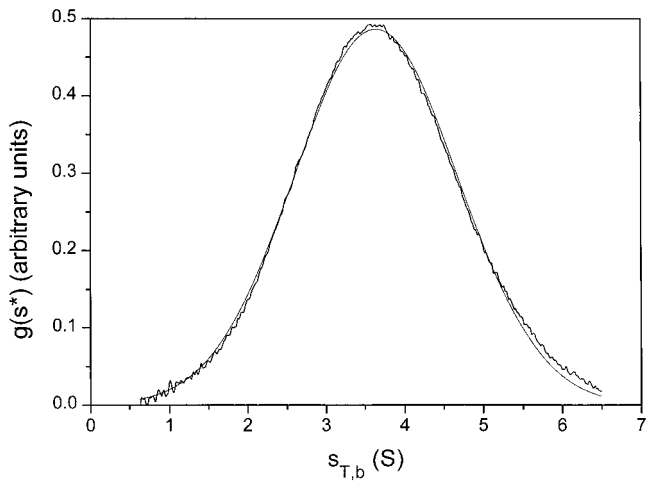

FIGURE 3 $g(s^*)$ versus $s_{T,b}$ plot from the program DCDT (Stafford, 1992) for B72.3 Fab′. Loading concentration of 1.10 mg/ml. Rotor speed = 49,000 rev/min, temperature = 20.0°C. $g(s^*)$ is the apparent (i.e., not corrected for diffusion) distribution of sedimentation coefficients. The thin line is a single Gaussian fit with peak $s_{T,b}$ = 3.63S.

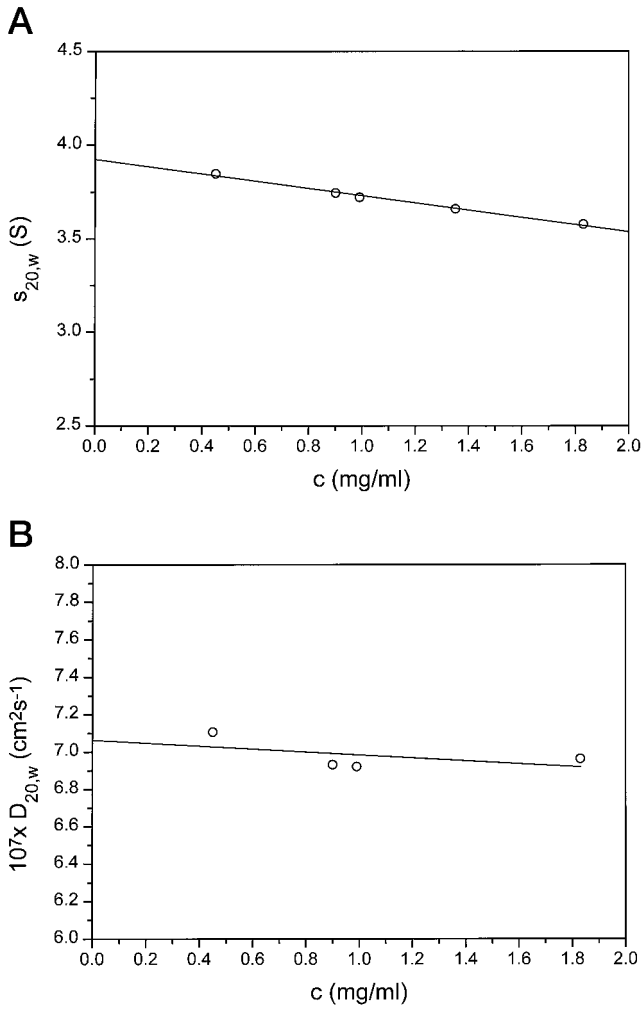

FIGURE 4 (*A*) Gralen plots of $s_{20,w}$ versus sedimenting concentration, *c* (corrected for radial dilution) for B72.3 Fab′. (*B*) Corresponding plot of $D_{20,w}$ versus *c*.

frictional coefficient f_o for a spherical particle of the same anhydrous volume as the particle (see Tanford, 1961).

f_o is simply the Stokes' law friction coefficient,

$$f_0 = 6\pi\eta a = 6\pi\eta\{(3\bar{v}M)/(4\pi N_A)\}^{1/3} \quad (6)$$

where η is the viscosity of the solution, a is the Stokes radius of the anhydrous particle, and v is the partial specific volume.

Thus from Eqs. 5 and 6, the frictional ratio f/f_o is given by

$$f/f_0 = M(1 - \bar{v}\rho)/[N_A 6\pi\eta s_{20,w}\{(3\bar{v}M)/(4\pi N_A)\}^{1/3}] \quad (7)$$

For B72.3c Fab′, if $\bar{v} = 0.727$ ml/g, $M = 47499$ g/mol, and $s^o_{20,w} = (3.92 \pm 0.01)$S, the frictional ratio $f/f_o = (1.22 \pm 0.01)$.

Estimation of the molecular hydration δ from f/f_o and P

The frictional ratio is related to the Perrin shape function P and the extent of hydration δ by the formula (see, e.g., Squire and Himmel, 1979):

$$f/f_0 = P\{1 + (\delta/\bar{v}\rho)\}^{1/3} \quad (8)$$

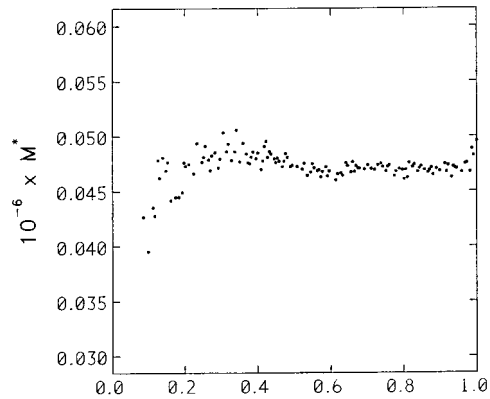

FIGURE 5 Sedimentation equilibrium M^* plot for the extraction of the molecular weight (whole cell weight average) for B72.3 Fab′: $M^*(\omega \rightarrow 1) = M_{w,app} = (47{,}000 \pm 2000)$ g/mol, and because of the low loading concentration, $M_{w,app} \approx M_w$. Rotor speed = 12,000 rev/min. Temperature = 20.0°C.

Taking $P = 1.0450$ corresponding to the semiaxial dimensions of the molecule from the crystal structure, we can estimate a value for the molecular hydration of "δ" = (0.43 ± 0.07) g H_2O/g protein. This value is "typical" compared to other globular proteins (Tanford, 1961; Zhou, 1995) and compares with a value of 0.37 g/g, which can be estimated from the amino acid sequence (Perkins, 1986). If we use instead the P value or 1.023 from the bead-shell model, the corresponding value for δ is (0.51 ± 0.07) g/g: this can be considered as an "apparent" hydration for the bead-shell approximation, which we denote as δ_{app}. A summary of these data is given in Table 4.

Comparison with deoxyhemoglobin and ribonuclease

Our value of (0.43 ± 0.07) for δ can be compared with values obtained in a similar way for other proteins. For example, an inertial ellipsoid fit to the crystal structure for deoxyhemoglobin yields axial ratios (a/b, b/c) of (1.27, 1.07). From ELLIPS2 this yields a value for the Perrin shape function P of 1.0071. Experimentally, the $s^o_{20,w}$ value is 4.6S (Behlke and Scheler, 1972). With $M = 64500$, $\bar{v} = 0.746$ ml/g, we obtain a frictional ratio $f/f_o = 1.174$. Combining f/f_o (Eq. 8) with P yields a value for the hydration δ of 0.44, almost identical to that for Fab′ and in exact agreement with a recently published value of 0.43, on the basis of thermodynamic nonideality and the algorithm COVOL (Harding et al., 1999).

For ribonuclease the inertial ellipsoid fit to the crystal structure yields (a/b, b/c) of (1.53, 1.23). From ELLIPS2 this yields a value for the Perrin shape function P of 1.0282. Experimentally, the $s^o_{20,w}$ value is 2.0S (see, e.g., Creeth, 1958). With $M = 13700$, $\bar{v} = 0.703$ ml/g we obtain a frictional ratio $f/f_o = 1.146$. Combining f/f_o (Eq. 8) with P yields a value for the hydration δ of 0.27, again in exact agreement with the recently published value of 0.25 on the basis of thermodynamic nonideality and the algorithm COVOL (Harding et al., 1999). Kumoninski and Pessen (1982) and Pessen et al. (1971) report a very similar value on the basis of low-angle x-ray scattering.

CONCLUDING REMARKS

We have shown that for a regular triaxial ellipsoidal structure based on the crystal dimensions of the Fab′ fragment of an antibody, only small errors are induced in the calculated set of hydrodynamic parameters if a prolate ellipsoid of revolution model is taken instead. A bead-shell model of

this ellipsoid of revolution reproduces the hydrodynamic parameters well, with the Perrin frictional-ratio base universal function returned with an accuracy better than ~2% within either the triaxial ellipsoid or the ellipsoid of revolution values, and all of the other parameters reproduced favorably, thus validating the bead-shell approximation to structures of this type. Furthermore, by combination of the value evaluated for the Perrin shape function P with the experimentally measured frictional ratio we have been able to obtain an estimate for both the hydration and the "apparent hydration" for the bead-shell model, a value that will subsequently prove useful for further modeling of intact, immunologically active antibody molecules, in which the bead-shell rather than ellipsoid-based modeling strategies are appropriate. It is hoped that such an approach will complement the advances that are now being made in structural determinations by x-ray methods of intact, immunologically active antibody molecules in the crystallized state (Harris et al., 1998a,b).

We thank Prof. Janet M. Thornton FRS, Prof. D. J. Winzor, and Dr. J. M. Creeth for helpful discussions.

REFERENCES

Ban, N., C. Excobar, K. W. Hasel, J. Day, and A. Greenwood. 1995. Structure of an antiidiotypic fab against feline peritoni virus-neutralizing antibody and a comparison with the complexed Fab. *FASEB J.* 9:107–114.

Banfield, M. J., D. J. King, A. Mountain, and R. K. Brady. 1997. VL:VH domain rotations in engineered antibodies: crystal structures of the Fab fragments from two murine anti-tumour antibodies and their engineered constructs. *Proteins Struct. Funct. Genet.* 29:161–171.

Behlke, J., and O. Ristau. 1997. Molecular mass determination by sedimentation velocity experiments and direct fitting of the concentration profiles. *Biophys. J.* 72:428–434.

Behlke, J., and W. Scheler. 1972. Der einfluss von Sauerstoff auf die reversible Spaltung des menschlichen Desoxyhamoglobins im elektrolytarmen Milieu. *Acta Biol. Med. Ger.* 28:K1–K4.

Bloomfield, V. A., W. O. Dalton, and K. E. van Holde. 1967. Frictional coefficients of multisubunit structures. *Biopolymers.* 5:135–148.

Brady, R. L., D. J. Edwards, R. E. Hubbard, J.-S. Juang, S. M. Lange, S. M. Roberts, R. J. Todd, J. R. Adair, J. S. Emtage, D. J. King, and D. C. Low. 1992. Crystal structure of a chimaeric Fab′ fragment of an antibody binding tumour cells. *J. Mol. Biol.* 227:253–264.

Byron, O. 1992. Solution studies on the conformation and assembly of the monoclonal antibody B72.3. Ph.D. dissertation. University of Nottingham.

Carrasco, B. 1998. Propiedades de macromoleculas rigidas en disolucion: modelos, methodos, computacionales y analisis de los datos experimentales. Ph.D. thesis. Universidad de Murcia.

Carrasco, B., and J. Garcia de la Torre. 1999. Hydrodynamic properties of rigid particles: comparison of different modeling and computational procedures. *Biophys. J.* 76:3044–3057.

Cölfen, H., and S. E. Harding. 1997. MSTARA and MSTARI: interactive PC algorithms for simple, model independent evaluation of sedimentation equilibrium data. *Eur. Biophys. J.* 25:333–346.

Creeth, J. M. 1958. Studies of free diffusion in liquids with the Rayleigh method. III. The analysis of known mixtures and some preliminary investigations with proteins. *J. Phys. Chem.* 62:66–74.

Creeth, J. M., and S. E. Harding. 1982. Some observations of a new type of point average molecular weight. *J. Biochem. Biophys. Methods.* 7:25–34.

Garcia de la Torre, J. 1989. Hydrodynamic properties of macromolecular assemblies. *In* Dynamic Properties of Biomolecular Assemblies. S. E. Harding and A. J. Rowe, editors. Royal Society of Chemistry, Cambridge, England. 3–31.

Garcia de la Torre, J., and V. A. Bloomfield. 1977. Hydrodynamic properties of macromolecular complexes. *Biopolymers.* 16:1747–1763.

Garcia de la Torre, J., and V. A. Bloomfield. 1981. Hydrodynamic properties of complex, rigid, biological macromolecules: theory and applications. *Q. Rev. Biophys.* 14:81–139.

Garcia de la Torre, J., and B. Carrasco. 1998. Intrinsic viscosity and rotational diffusion of bead models for rigid macromolecules and bioparticles. *Eur. Biophys. J.* 27:549–557.

Garcia de la Torre, J., B. Carrasco, and S. E. Harding. 1997. SOLPRO: theory and computer program for the prediction of solution properties of rigid macromolecules and bioparticles. *Eur. Biophys. J.* 25:361–372.

Garcia de la Torre, J., S. E. Harding, and B. Carrasco. 1999. Calculation of NMR relaxation, covolume, and scattering-related properties of bead models using the SOL-PRO computer program. *Eur. Biophys. J.* 28: 119–132.

Garcia de la Torre, J., and V. Rodes. 1983. Effects from bead size and hydrodynamic interactions on the translational and rotational coefficients of macromolecular bead models. *J. Chem. Phys.* 79:2454–2460.

Giebeler, R. 1992. The Optima XL-A: a new analytical ultracentrifuge with a novel precision absorption optical system. *In* Analytical Ultracentrifugation in Biochemistry and Polymer Science. S. E. Harding, A. J. Rowe, and J. C. Horton, editors. Royal Society of Chemistry, Cambridge, England.

Gralen, N. 1944. Sedimentation and diffusion measurements on cellulose and cellulose derivatives. Ph.D. dissertation. University of Uppsala.

Green, A. A. 1933. The preparation of acetate and phosphate buffer solutions of known pH and ionic strength. *J. Am. Chem. Soc.* 55: 2331–2336.

Hanisch, F. G., G. Uhlenbruck, H. Egge, and J. Peter-Katalinic. 1989. A B72.3 second generation monoclonal antibody CC49 defines the mucin carried carbohydrate epitope Galβ(1–3)[NeuAcα(2–6)]GalNAc. *Biol. Chem. Hoppe-Seyler.* 370:21–26.

Harding, S. E. 1989. Modelling the gross conformation of assemblies using hydrodynamics: the whole body approach. *In* Dynamic Properties of Biomolecular Assemblies. S. E. Harding and A. J. Rowe, editors. Royal Society of Chemistry, Cambridge, England. 32–56.

Harding, S. E., J. C. Horton, and H. Cölfen. 1997. The ELLIPS suite of macromolecular conformation algorithms. *Eur. Biophys. J.* 25:347–359.

Harding, S. E., J. C. Horton, S. Jones, J. M. Thornton, and D. J. Winzor. 1999. COVOL: an interactive program for evaluating second virial coefficients from the triaxial shape or dimensions of rigid macromolecules. *Biophys. J.* 76:2432–2438.

Harding, S. E., and P. Johnson. 1985a. The concentration dependence of macromolecular parameters. *Biochem. J.* 231:543–547.

Harding, S. E., and P. Johnson. 1985b. Physicochemical studies on turnip-yellow-mosaic virus. *Biochem. J.* 231:549–555.

Harding, S. E., and A. J. Rowe. 1982a. Modelling biological macromolecules in solution. 1. The ellipsoid of revolution. *Int. J. Biol. Macromol.* 4:160–164.

Harding, S. E., and A. J. Rowe. 1982b. Modelling biological macromolecules in solution. 3. The L-R intersection method for triaxial ellipsoids. *Int. J. Biol. Macromol.* 4:357–361.

Harding, S. E., and A. J. Rowe. 1983. Modelling biological macromolecules in solution. II. The general triaxial ellipsoid. *Biopolymers.* 22: 1813–1829 and 23:843.

Harris, L. J., S. B. Larson, E. Skaletsky, and A. McPherson. 1998a. Comparison of the conformations of two monoclonal antibodies with hinges. *Immunol. Rev.* 163:35–43.

Harris, L. J., E. Skaletsky, and E. McPherson. 1998b. Crystallographic structure of an intact IgG1 monoclonal antibody. *J. Mol. Biol.* 275: 861–872.

Hubbard, S. 1994. PROTRUDER: A FORTRAN Program to Calculate an Equi-momental Ellipsoid and Make Protrusion Index Calculations. University College, London.

King, D. J., J. R. Adair, S. Angal, D. C. Low, K. A. Proudfoot, J. C. Lloyd, M. W. Dodmer, and G. T. Yarranton. 1992. Expression, purification and

characterization of a mouse-human chimeric antibody and chimeric Fab′ fragment. *Biochem. J.* 281:317–323.

Kumoninski, T. F., and H. Pessen. 1982. Estimation of sedimentation coefficients of globular proteins: an application of small-angle x-ray scattering. *Arch. Biochem. Biophys.* 219:89–100.

Laskowski, R. A. 1995. SURFNET: a program for visualizing molecular surfaces, cavities and intermolecular interactions. *J. Mol. Graph.* 13: 323–330.

MacMillan, W. D. 1936. Dynamics of Rigid Bodies. McGraw-Hill, New York. 31–52.

Perkins, S. J. 1986. Protein volumes and hydration effects. The calculations of partial specific volumes, neutron scattering matchpoints and 280 nm absorption coefficients for proteins and glycoproteins from amino acid sequences. *Eur. J. Biochem.* 157:169–180.

Perrin, F. 1934. Mouvement Brownian d'un ellipsoide. I. Dispersion dielectrique pour des molecules ellipsoidales. *J. Phys. Radium.* 5:497–511.

Perrin, F. 1936. Mouvement Brownian d'un ellipsoide. II. Rotation libre et depolarisation des fluorescences. Translation et diffusion de molecules ellipsoidales. *J. Phys. Radium.* 7:1–11.

Pessen, H., T. F. Kumoninski, and S. N. Timasheff. 1971. The use of small-angle x-ray scattering to determine protein conformation. *J. Agric. Food Chem.* 19:698–702.

Philo, J. S. 1997. An improved function for fitting sedimentation velocity data for low-molecular-weight solutes. *Biophys. J.* 72:435–444.

Saul, F. A., and R. J. Poljak. 1992. Crystal structure of human-immunoglobulin fragment refined at 2.0-Angstrom resolution. *Proteins Struct. Funct. Genet.* 14:363–371.

Schachman, H. K. 1959. Ultracentrifugation in Biochemistry. Academic Press, New York.

Simha, R. 1940. The influence of Brownian motion on the viscosity of solutions. *J. Phys. Chem.* 44:25–34.

Squire, P. G., and M. E. Himmel. 1979. Hydrodynamics and protein hydration. *Arch. Biochem. Biophys.* 196:165–177.

Stafford, W. F. 1992. Methods for obtaining sedimentation coefficient distributions. *In* Analytical Ultracentrifugation in Biochemistry and Polymer Science. S. E. Harding, A. J. Rowe, and J. C. Horton, editors. Royal Society of Chemistry, Cambridge, England. 359–393.

Svedberg T., and Pedersen, O. 1990. The ultracentrifuge. Oxford University Press, Oxford.

Synge, J. L., and B. A. Griffin. 1959. Principles of Mechanics. McGraw-Hill, New York. 282–294.

Tanford, C. 1961. Physical Chemistry of Macromolecules. J. Wiley and Sons, New York.

Taylor, W. R., J. M. Thornton, and W. G. Turnell. 1983. An ellipsoidal approximation of protein shape. *J. Mol. Graph.* 1:30–38.

Zhou, H.-X. 1995. Calculation of translational friction and intrinsic viscosity. II. Application to globular proteins. *Biophys. J.* 69:2298–2303.